Grid Telescoping in Numerical Weather Prediction

G. E. HILL[1]

Air Force Cambridge Research Laboratories, Bedford, Mass.

(Manuscript received 28 July 1967, in revised form 11 September 1967)

ABSTRACT

A technique is presented as a means of treating problems in meteorology by numerical prediction on a fine scale. The method involves solution of numerical equations on a grid of data points in the usual way. Then, results from that forecast are used for the boundary conditions of a more dense but smaller-size grid network placed within the original one. Successively smaller grids are introduced so that the final grid size is as small as desired.

Twenty-four hour forecasts have been made with a 2-level baroclinic model using a grid spacing reduced from 655 km to 327 km, to 163 km, and finally to 81 km. For an initial test, the method is applied to a developing cyclone just off the East Coast of the United States. During the 24-hr period of forecast, this cyclone developed from an incipient stage to a mature occluding system. The results of the numerical forecasts show that the method may be used successfully.

1. Introduction

Large-scale atmospheric motions have been intensively studied in the past two decades by numerical integration of equations of motion and heat. These equations are expressed in finite-difference form, the continuous variables being represented by values at a finite number of suitably spaced points and derivatives being represented by differences between values at nearby points. By integration of these equations, 24–72 hr forecasts of basic parameters such as pressure-height, vorticity and vertical motion have been made for both research and operational purposes.

An early attempt (Richardson, 1922) to produce a numerical forecast was a failure. In Richardson's work, sound and gravity waves were not eliminated from possible solutions, and with the time step used, the Courant *et al.* (1928) stability criterion, though not yet known, was violated. Even had these waves been eliminated, his time-space grid was unsuitable for stable integrations.

The first successful attempt at numerical integration of the equations governing large-scale atmospheric motions was carried out by Charney *et al.* (1950) who integrated a vorticity equation over a 24-hr period. In this work the stability criterion and filtering requirements were taken fully into account. Since then, many atmospheric models have been devised, some in which the quasi-geostrophic assumption of Charney's model is not required, others in which additional vertical resolution is added.

Recently, considerable emphasis has been placed on integration of the primitive equations. Such integrations are in the first instance simple, but in practice they require relatively small time steps, and apparently also require rather complicated smoothing operators.

If we consider the earlier models, i.e., those involving vorticity equations, we find that the degree of space-time resolution has been largely a matter of computer technology. The core storage available when Charney carried out his integrations for a single-level model was so small that he was restricted to a grid of 270 points. To make the area of forecast large enough to be of meteorological interest, a grid-space interval of 736 km was used.

In Thompson and Gates' (1956) two-level model a grid of 414 points was used along with a grid-space interval of 278 km. Twenty-four hour forecasts of 500- and 1000-mb height and 500-mb vertical motion were made on an IBM 701 for a large number of cases. These forecasts required about a half hour for the computations. For boundary conditions Thompson used the observed 24-hr changes which were assumed to occur at an even rate during the period.

With recognition of the boundary value problem, an octagonal grid covering most of the Northern Hemisphere was introduced in the Joint Numerical Weather Weather Prediction Unit [see Thompson (1961)]. The boundaries of such a grid lie in low latitudes where changes are relatively small, and also at a large distance from middle latitude weather systems.

Recently, Howcroft (1966) has developed a "fine-mesh limited area forecasting model" for operational use. In this limited area the grid spacing and time step are half those of the hemispheric grid.

In the present work we demonstrate a method which we refer to as "grid telescoping," whereby forecasts are

[1] Present affiliation: Lowell Technological Institute, Lowell, Mass.

made first for a hemispheric grid, and then for several successively smaller grids. The final grid may be a few tens of kilometers, though this lower limit has not been established. It may well depend upon the model itself and upon the initial data. If a grid spacing of 40 km, for example, were used throughout the entire region, over 150,000 points per level would be required. Even if computer storage capacity were sufficient, the data preparation and computation time to complete a forecast would not be feasible.

In the grid telescoping method, a numerical integration is carried out for an octagonal hemispheric grid as usual. Then another grid, preferably of the same shape and number of points, but of half the grid-point spacing, is placed within the original grid so that about a quarter of the points of each grid coincide. Forecasts are made for each grid separately, except for the boundary of the second grid. When data is required there, it is obtained directly from the original grid when the points coincide and by interpolation when they do not.

The forecast area will be reduced to one-quarter of the original. In making a forecast it is necessary to halve the time step as well. In such a case, data on all of the boundary points for the intermediate time step, $\tau+\frac{1}{2}$, is obtained by interpolation between time step τ and $\tau+1$. Such a process may be repeated by placing a third grid of appropriate size and dimensions on the second grid and so on.

Grid telescoping makes feasible a numerical forecast on a much smaller size scale than is presently available without greatly increasing computer storage or computation time. Furthermore, the preparation of initial data for the method, though increased, remains feasible. The method may be applied to any model and ostensibly has its chief advantage in the forecast of small-scale cyclones, mesoscale features such as squall lines, and orographic effects not yet adequately treated.

To test the merits of the idea outlined above we will develop a simple two-level model, construct a set of grids and numerically integrate the forecast equations for a particular case.

2. Test model

a. General equations.

The equations governing quasi-hydrostatic atmospheric motion in an x, y, p, t coordinate system are

$$\frac{\partial z}{\partial p}=-\frac{RT}{Pg}, \tag{1}$$

$$\frac{du}{dt}=fv-g\frac{\partial z}{\partial x}, \tag{2}$$

$$\frac{dv}{dt}=-fu-g\frac{\partial z}{\partial y}, \tag{3}$$

where

$$\frac{d}{dt}\equiv\frac{\partial}{\partial t}+u\frac{\partial}{\partial x}+v\frac{\partial}{\partial y}+\omega\frac{\partial}{\partial p}, \tag{4}$$

$$\omega\equiv\frac{dp}{dt}, \tag{5}$$

and where u is the horizontal wind velocity component toward the x direction, v the horizontal wind velocity component toward the y direction, f the Coriolis parameter, z height above sea level of a constant pressure surface, T temperature, and P pressure.

If the motion takes place adiabatically, the first law of thermodynamics may be written

$$\frac{dT}{dt}=\frac{kT}{p}\omega \quad \text{or} \quad \frac{\partial T}{\partial t}+u\frac{\partial T}{\partial x}+v\frac{\partial T}{\partial y}+\sigma\omega=0, \tag{6}$$

where k is a constant equal to 0.288 and $\sigma=\partial T/\partial p-kT/p$. The equation of continuity is

$$\frac{\partial u}{\partial x}+\frac{\partial v}{\partial y}+\frac{\partial \omega}{\partial p}=0. \tag{7}$$

b. Model and modified equations.

By taking the curl of (2) and (3) we derive a vorticity equation. Neglecting the well-known twisting terms and the vertical transport of vorticity, we write with the aid of (7),

$$\frac{\partial \eta}{\partial t}+u\frac{\partial \eta}{\partial x}+v\frac{\partial \eta}{\partial y}=\eta\frac{\partial \omega}{\partial p}, \tag{8}$$

where

$$\eta=\zeta+f \quad \text{and} \quad \zeta=\frac{\partial v}{\partial x}-\frac{\partial u}{\partial y}. \tag{9}$$

Next, we find a relation between the wind and pressure-height field. For this purpose if the wind is considered to be nondivergent, we can define a stream function ψ such that

$$u=-\frac{\partial \psi}{\partial y} \quad \text{and} \quad v=\frac{\partial \psi}{\partial x}. \tag{10}$$

Using (9) and (10) along with the geostrophic relations, we obtain a simplified balance equation which is written for convenience in two forms:

$$\nabla^2\psi=\frac{g}{f}\nabla^2 z-\frac{g}{f^2}\nabla z\cdot\nabla f, \tag{11}$$

$$\nabla^2 z=\frac{f}{g}\nabla^2\psi+\frac{1}{g}\nabla\psi\cdot\nabla f. \tag{12}$$

To find an ω equation we combine (1) with an approximate form of (11) neglecting the dot-product term. This equation is differentiated with respect to time and

substituted appropriately into the vorticity equation differentiated with respect to pressure. Then by forming the Laplacian of (6), the time derivative of $\nabla^2 T$ is eliminated, leaving an equation in ω and its derivatives. In this equation the pressure variations of ω are neglected. The result is

$$\nabla^2\sigma\omega+\nabla^2\left(u\frac{\partial T}{\partial x}+v\frac{\partial T}{\partial y}\right)+\frac{fp}{R}\frac{\partial}{\partial p}\left(u\frac{\partial \eta}{\partial x}+v\frac{\partial \eta}{\partial y}\right)=0. \quad (13)$$

Such an equation is generally well known and the details of its derivation may be obtained from Thompson (1961).

To apply these equations we use a simple model atmosphere consisting of two levels, one at 500 mb and the other at 1000 mb. It is assumed that the divergence is zero at 500 mb, and the static stability σ is the same at 500 mb as it is between 500 and 1000 mb.

c. Finite difference equations.

Thus far the equations are expressed in the same form as in a Cartesian coordinate system, provided that appropriate values of the Coriolis parameter are used. To make use of this coordinate system, observed data are projected onto a polar stereographic map, true at 60N, whereupon a grid of data points is placed so that they are separated by equal distances parallel to the axes of a Cartesian coordinate system. Observed and projected distances are related by a map factor m.

In finite difference form the vorticity is written

$$\eta=\frac{m^2}{d^2}\nabla^2\psi+f, \quad (14)$$

where d is the grid spacing, and ∇^2 is the finite difference Laplacian operator.

The barotropic vorticity equation (500 mb) is

$$\nabla^2\frac{\partial\psi}{\partial t}+\tfrac{1}{4}J(\psi,\eta)=0, \quad (15)$$

where J is the finite difference Jacobian operator.

The 500-mb temperature equation is

$$\frac{\partial T}{\partial t}+\frac{m^2}{4d^2}J(\psi,T)+\sigma\omega=0. \quad (16)$$

The 500-mb ω equation is

$$\nabla^2\sigma\omega+\tfrac{1}{4}\nabla^2\frac{m^2}{d^2}J(\psi,T)+\frac{fp}{4R}J\left(\frac{\partial\psi}{\partial p},\eta\right)+\frac{fp}{R}J\left(\psi,\frac{m^2}{d^2}\nabla^2\frac{\partial\psi}{\partial p}\right)=0. \quad (17)$$

The balance equations are given in geostrophic form:

$$\nabla^2\psi=\frac{g}{f}\nabla^2 z-\frac{g}{4f^2}\nabla z\cdot\nabla f, \quad (18)$$

$$\nabla^2 z=\frac{f}{g}\nabla^2\psi+\frac{1}{4g}\nabla\psi\cdot\nabla f. \quad (19)$$

Differentiating (18) with respect to p and using the hydrostatic relation, we have

$$\nabla^2\frac{\partial\psi}{\partial p}=-\frac{R}{fp}\nabla^2 T+\frac{R}{4f^2p}\nabla T\cdot\nabla f, \quad (20)$$

where ∇ is the finite-difference gradient operator, and T and p may be taken at the 500-mb surface or an average between 500 and 1000 mb depending upon where $\partial\psi/\partial p$ is required. Finally, the 1000-mb temperature equation is

$$\frac{\partial T}{\partial t}+\frac{m^2}{4d^2}J(\psi,T)=0, \quad (21)$$

where ψ and T refer, of course, to the 1000-mb stream function and temperature.

Eqs. (14)-(21) form a complete system from which time changes of the dependent variables are found. Equations for ψ and T at 500 mb and T at 1000 mb are prognostic and the remaining are diagnostic. The prognostic equations are treated in the usual way, i.e., for the first time step we use a noncentered difference over one time step and subsequently we use centered time differences.

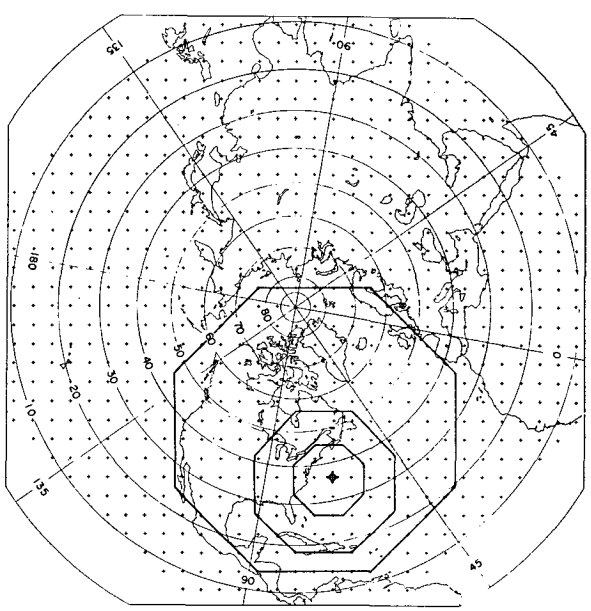

FIG. 1. Octagonal grids.

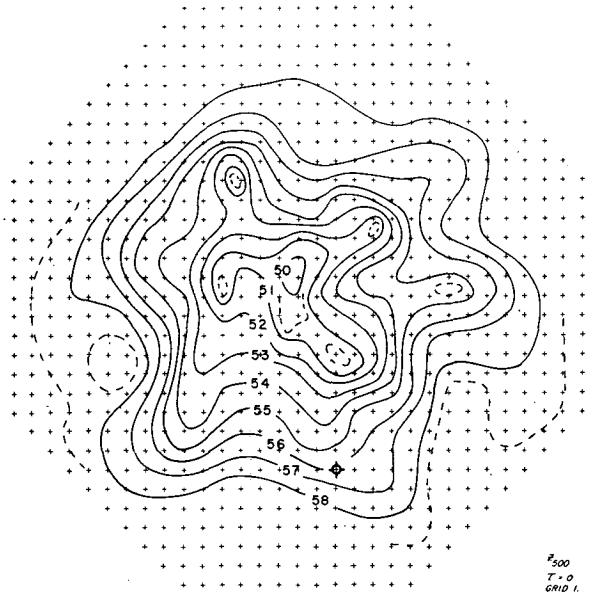

FIG. 2. Initial 500-mb height, grid 1.

Several equations in this system are Poisson; they are solved by the Liebmann relaxation technique with a relaxation coefficient of 0.43.

d. Application.

1) Octagonal grid. Numerical prediction of the dependent variables is first carried out with an octagonal grid covering most of the Northern Hemisphere. The grid, shown in Fig. 1, is a square 31×31 minus 45 points on each corner so that the octagonal grid has a total of 781 points, of which 697 are interior points. The grid spacing is set equal to 655 km and the time step is 1 hr.

Data measured or predicted over the grid are as follows.

Initial fields:

θ	latitude of grid point
Z_{500}	500-mb height
T_{500}	500-mb temperature
$Z_{500}-Z_{1000}$	500 to 1000 mb thickness

Derived initial fields:

T_{1000}	1000-mb temperature
Z_{1000}	1000-mb height

Forecast fields by time integrations:

ψ_{500}	500-mb stream function
T_{500}	500-mb temperature
T_{1000}	1000-mb temperature

Forecast fields from diagnostic equations:

ψ_{1000}	1000-mb stream function
$(\sigma\omega)_{500}$	500-mb $\sigma\omega$

Additional forecast fields from diagnostic equations (used for subgrid boundaries):

Z_{500}	500-mb height
Z_{1000}	1000-mb height

The pressure height fields Z_{500} and Z_{1000} are also of interest at the forecast intervals.

Boundary conditions for the hemispheric octagonal grid are as follows:

1. $Z=$constant
2. $\psi=$constant (a streamline is coincident with the boundary)
3. $T=$constant (an isotherm is coincident with the boundary)
4. $\omega=0$
5. $J(\psi,T)=0$
6. $\partial\psi/\partial t=0$ (from conditions 2, 3 and 4).
7. $\partial T/\partial t=0$
8. $\nabla^2\psi=0$
9. $\nabla^2 T=0$

Adjusting and smoothing of initial data on the hemispheric grid are employed so that the boundary value is constant, and two-grid interval variations are eliminated. Also, spurious vorticity concentrations are removed from low latitudes by the adjusting and smoothing.

Adjusting is accomplished by setting the Laplacian of ψ and T equal to zero on the outer two rows of the hemispheric grid and one-quarter of its value on the third row, one-half on the fourth row, and three-quarters on the fifth row. The remaining interior is unchanged. Then the field is relaxed and the new values found. They differ from the original only near the boundary which becomes "soft."

A 25-point smoothing operator (Shuman, 1957) is applied to all points on the hemispheric grid except the outer two rows. With smoothing, two-grid interval variations are removed, the longer waves are only

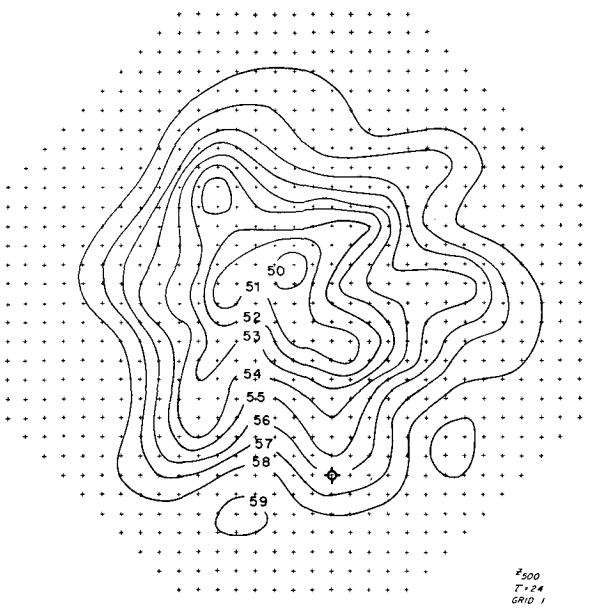

FIG. 3. 24-hr forecast 500-mb height, grid 1.

affected slightly, and the eight grid-interval variations are unaffected.

2) Second grid. The second grid is an octagonal one of 31×31 points. It is placed within the original octagonal grid in a way such as that shown in Fig. 1. The boundary conditions for the second grid are found from the original grid either by taking data directly or by interpolating it. The interpolation is made on the basis of the second derivative.

To show how interpolated values of ψ, for example, are found, consider four points of the octagonal grid which lie on a boundary of the second grid. Values of ψ are known at these points and ψ is required midway between the second and third points. In finite difference form (with the map factor equal to unity) the second derivative at i is

$$\left(\frac{\partial^2\psi}{\partial x^2}\right)_i=\frac{1}{d^2}(\psi_{i+1}+\psi_{i-1}-2\psi_i), \tag{22}$$

and at $i+1$ is

$$\left(\frac{\partial^2\psi}{\partial x^2}\right)_{i+1}=\frac{1}{d^2}(\psi_{i+2}+\psi_i-2\psi_{i+1}). \tag{23}$$

Linear interpolation gives

$$\left(\frac{\partial^2\psi}{\partial x^2}\right)_{i+\frac{1}{2}}=\frac{1}{2d^2}(\psi_{i+2}+\psi_{i-1}-\psi_i-\psi_{i+1}). \tag{24}$$

Writing the second derivative at $i+\frac{1}{2}$ directly, we have

$$\left(\frac{\partial^2\psi}{\partial x^2}\right)_{i+\frac{1}{2}}=\frac{1}{d^2/4}(\psi_{i+1}+\psi_i-2\psi_{i+\frac{1}{2}}). \tag{25}$$

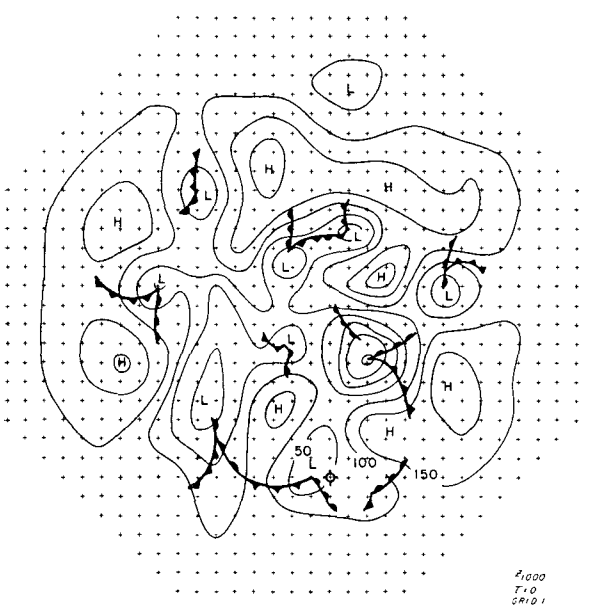

FIG. 4. Initial 1000-mb height, grid 1.

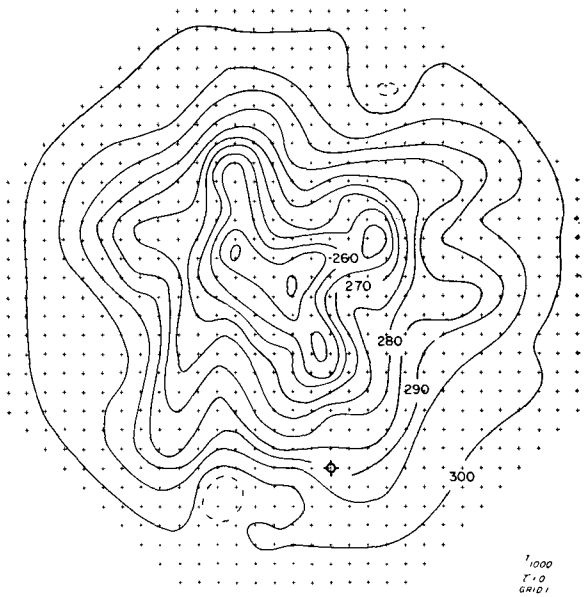

FIG. 5. Initial 1000-mb temperature, grid 1.

Equating the two forms of $(\partial^2\psi/\partial x^2)_{i+\frac{1}{2}}$ and solving for $\psi_{i+\frac{1}{2}}$ we obtain

$$\psi_{i+\frac{1}{2}}=\tfrac{1}{16}[q(\psi_{i+1}+\psi_i)-(\psi_{i+2}+\psi_{i-1})]. \tag{26}$$

For this grid both the grid spacing and the time step are one-half that of the original grid, i.e., 327.5 km and one-half hour, respectively. Thus, data for the half-hour steps must be interpolated on the boundaries of the second grid from the octagonal grid.

The initial temperature, thickness or height fields may be either interpolated or found directly from analyzed charts. It should be noted that if analyzed data are used, the effects of errors on height or tempera-

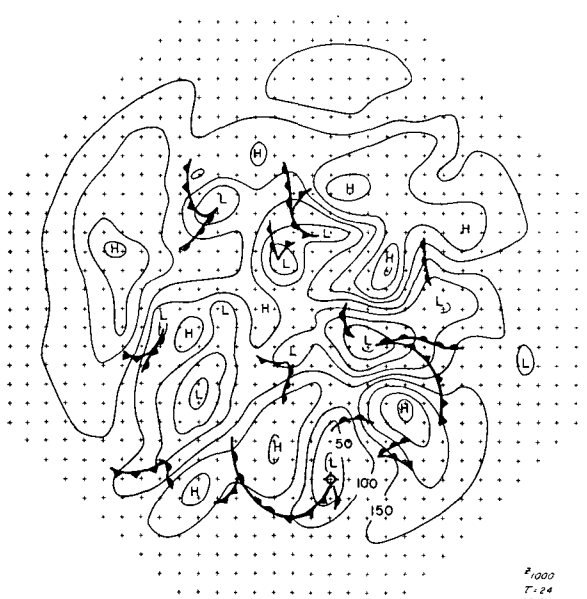

FIG. 6. 24-hr forecast 1000-mb height, grid 1.

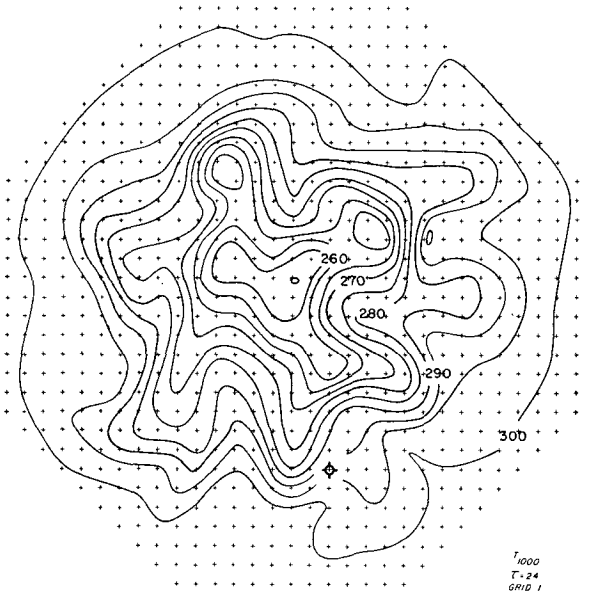

FIG. 7. 24-hr forecast 1000-mb temperature, grid 1.

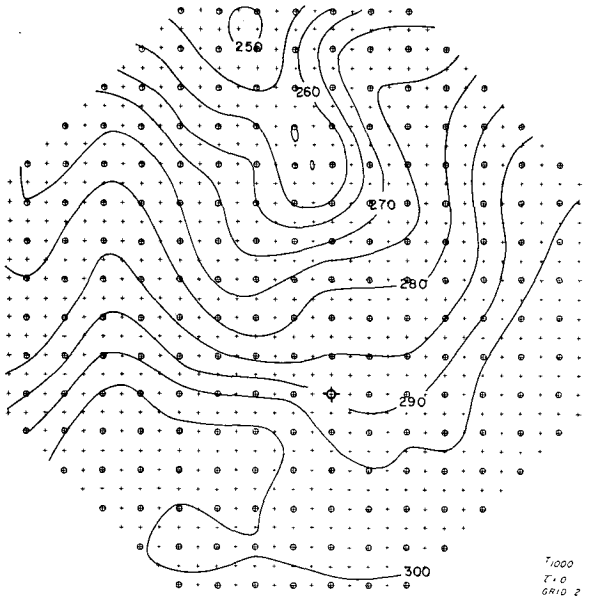

FIG. 9. Initial 1000-mb temperature, grid 2.

ture gradients increase as the grid distance decreases. Thus, it is not clear whether analyzed initial data would lead to better results than interpolated initial data.

Interpolated fields serve another purpose than to specify boundary or initial conditions, that is, the interpolated fields may be used as an initial guess required in the relaxation process. It has not been determined whether solutions are obtained faster by using interpolated fields or by using estimated fields based on previous time steps.

No adjusting is made for data from the smaller grids, and smoothing is applied at 12 and 24 hr only. Again, the smoothing is applied to all points within the grid except the outer two rows. The outer row of data is obtained, as described before, from the next larger grid. The second row is smoothed by interpolating so that the second derivative normal to the grid boundary is equal to that derivative at the third row. An alternative to this latter procedure would be to save an additional row of data from the larger grid and then smooth all of the grid of interest except for the boundary.

During the course of numerical integration, spatial oscillations tended to develop near the boundaries in regions of outflow. These disturbances were successfully controlled by the smoothing.

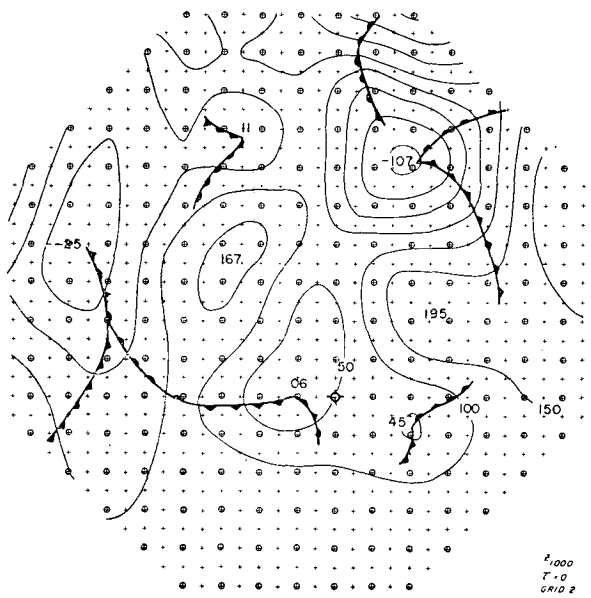

FIG. 8. Initial 1000-mb height, grid 2.

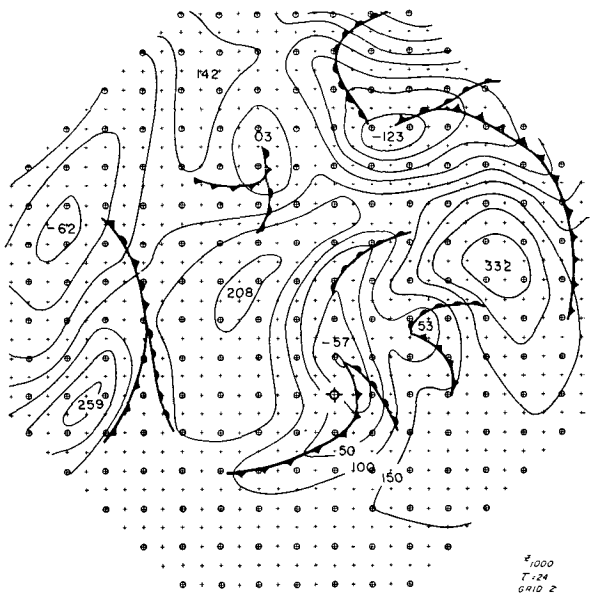

FIG. 10. 24-hr forecast 1000-mb height, grid 2.

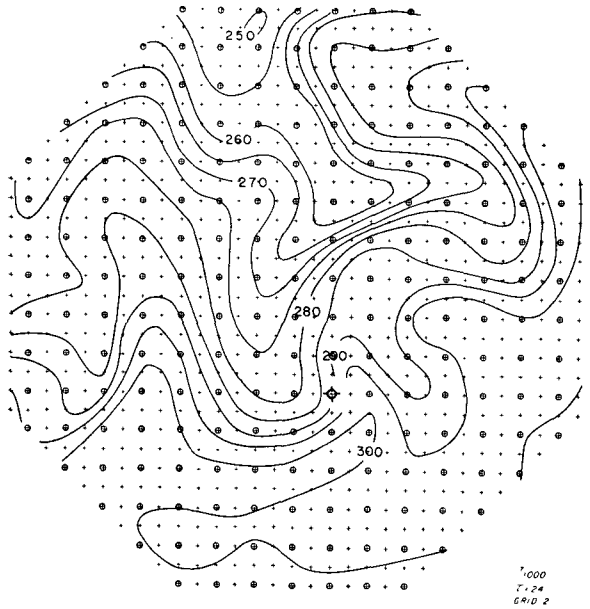

FIG. 11. 24-hr forecast 1000-mb temperature, grid 2.

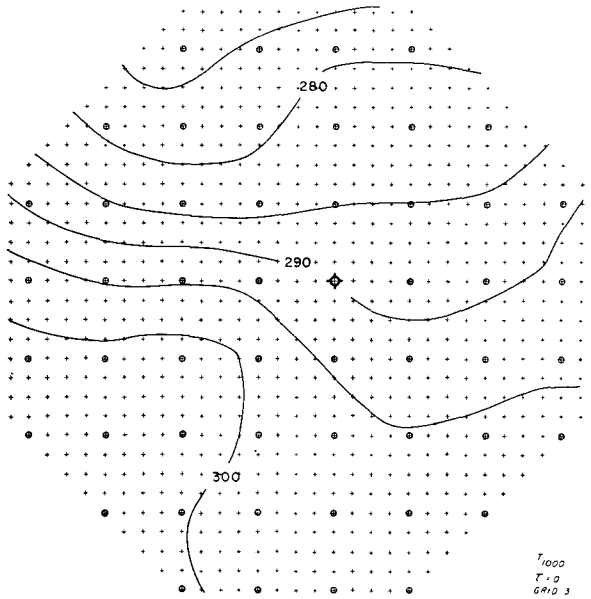

FIG. 13. Initial 1000-mb temperature, grid 3.

3) Subsequent grids. The process described above for the second grid may be repeated so that the grid spacing and time step become smaller. For the third grid the spacing becomes 163.75 km and the time step $\frac{1}{4}$ hr; for the fourth grid we have 81.875 km and $\frac{1}{8}$ hr, respectively.

3. Test case

Data used to test the model were obtained from charts at 1200 GMT 9 April 1965. Grid telescoping down to an 81-km mesh was directed into a developing cyclone just off the East Coast of the United States. During the subsequent 24 hr this cyclone developed from an incipient disturbance to a mature occluding system; the central pressure dropped from about 998 to 982 mb as it moved eastward. In what follows, these features are approximately reproduced by using grid telescoping with four grids including the hemispheric one.

In Figs. 2 and 3 the 500-mb height is shown for $\tau=0$ and the (barotropic) forecast for $\tau=24$ hr, respectively. We notice especially the trough-ridge-trough pattern over North America and the eastward movement of this pattern over the 24-hr period.

In Figs. 4-19 we show the initial and 24-hr forecast

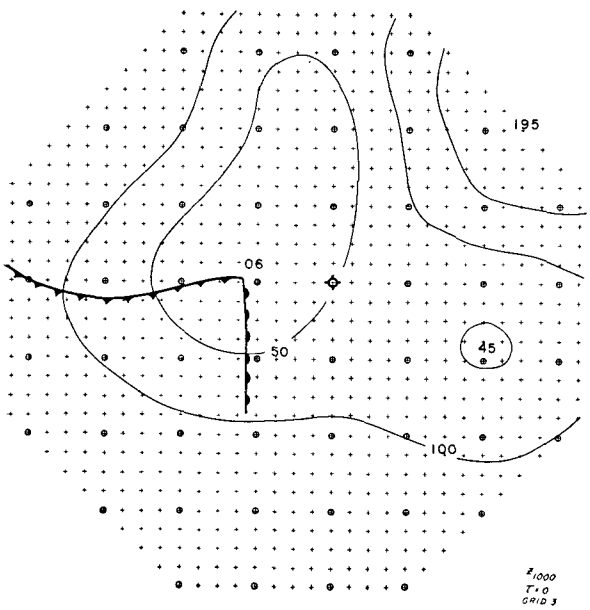

FIG. 12. Initial 1000-mb height, grid 3.

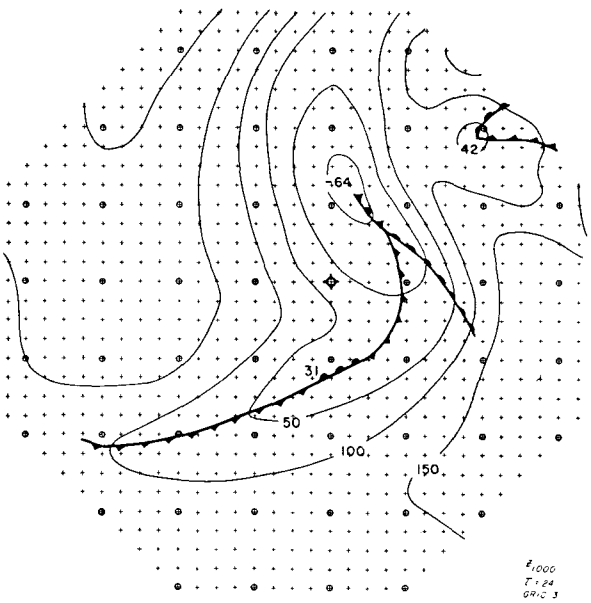

FIG. 14. 24-hr forecast 1000-mb height, grid 3.

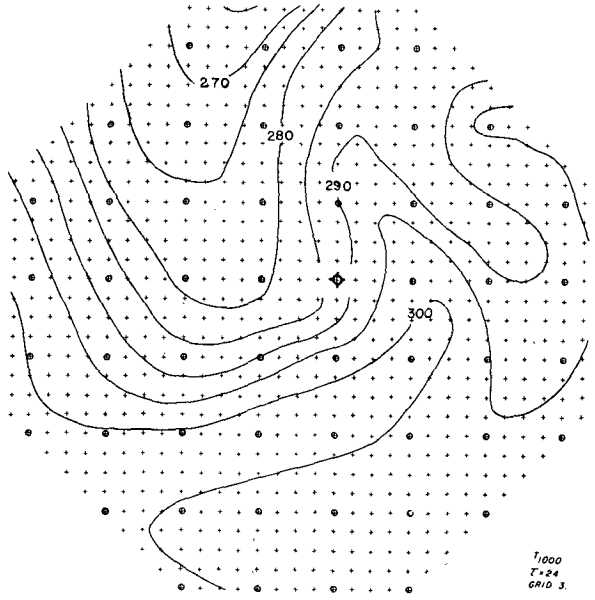

FIG. 15. 24-hr forecast 1000-mb temperature, grid 3.

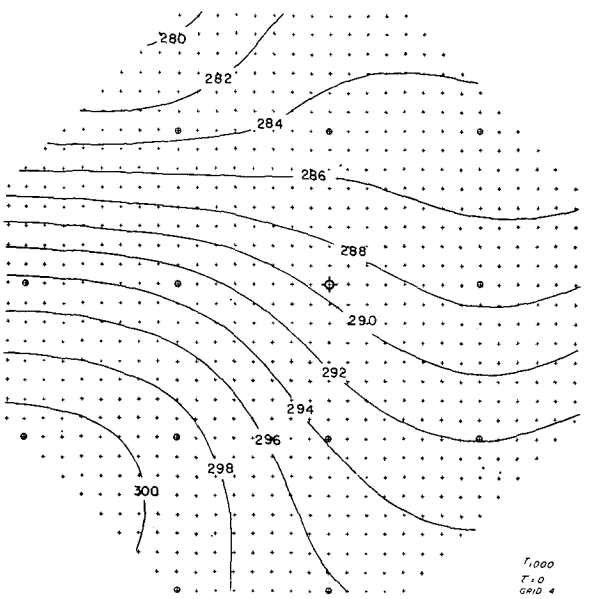

FIG. 17. Initial 1000-mb temperature, grid 4.

fields of 1000-mb height and temperature; there are four sets of such figures, one set for each grid. On the first set (Figs. 4-7), the contours on the 1000-mb charts are drawn every 50 m and the centers are marked with an H or an L. Only a few contours are labelled for the sake of clarity. The 1000-mb temperature maps are drawn for intervals of 5K.

The relative smoothness of the 1000-mb temperature field arises by the fact that the initial temperature is not observed, but is derived. It is found by computing what temperature would satisfy a linear relationship, using the hydrostatic equation, between the temperature at 500 mb, and the observed 500-1000 mb thickness.

The frontal systems shown on the 1000-mb height charts are those found from a comparison between the 1000-mb height fields and the temperature fields shown here. The criterion used is that generally a front passes through a low center, that the type of front, whether cold or warm, depends upon the sign of the temperature advection, that the fronts tend to lie in troughs, and that the front marks the boundary of strong temperature advection unless it is stationary or occluded.

Since we are primarily concerned with the telescoping method, we will confine our discussion to the systems within the second grid at least.

On the initial 1000-mb hemispheric chart we see near

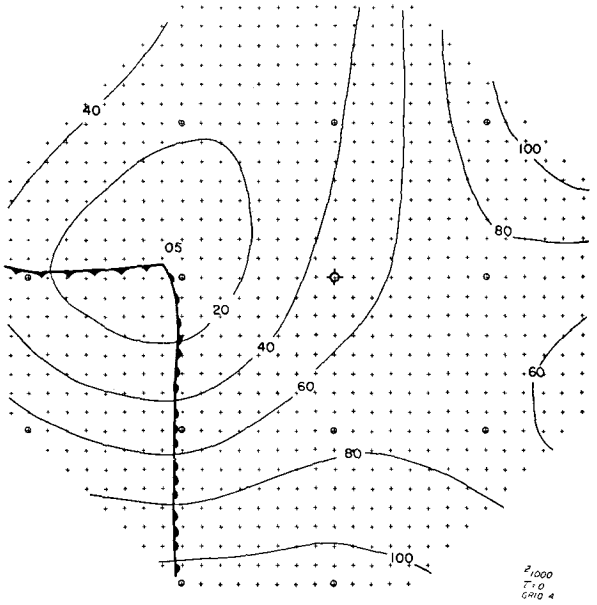

FIG. 16. Initial 1000-mb height, grid 4.

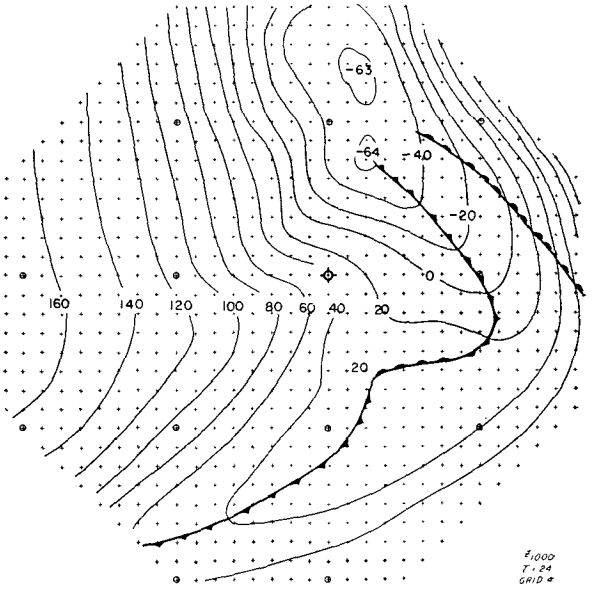

FIG. 18. 24-hr forecast 1000-mb height, grid 4.

Iceland a deep low which moves northeastward during the 24-hr forecast period. To the southwest a strong high is generated. The low off the United States East Coast moves eastward, while the smaller low farther off the coast moves north-northeastward. The high over Canada moves southward and another high is generated in northern Mexico. Finally a low on the Pacific Coast remains nearly stationary and a portion of it regenerates to the west. The thermal wave pattern shows an intensification in the Atlantic and in the eastern United States. We note especially the surge of cold air southward in the eastern United States.

On the second set (Figs. 8-11) the central value of the highs and lows are indicated. The contour intervals are the same as before i.e., every 50 m and 5K. Here we see some interesting details—the low just off the United States East Coast deepens 63 m and is shown to move northeastward instead of eastward. The small low nearby fills slightly and moves northward. The high over Canada moves only slightly southward while intensifying. The Icelandic low has a more northerly course than on grid 1. The low on the Pacific Coast retrogrades some.

The occluding process is evident in three of the lows—the one near Iceland, the one off the United States East Coast and the small one farther east. The thermal pattern renders these features clearly.

On the third set (Figs. 12-15) our attention is directed toward the U. S. East Coast low center and the smaller one nearby. Now we see the movement of the intensifying low to be northeastward. It deepens by 70 m, with a small, somewhat stable looking low appearing on the trailing cold front. The main low shows the occluding process as evident by the marked thermal wave development. The small low to the east shows a movement

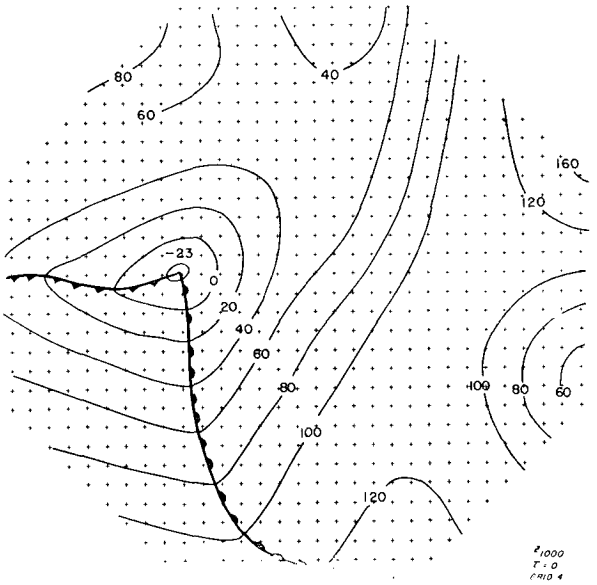

FIG. 20. Observed initial ($\tau=0$) 1000-mb height, grid 4.

almost due northward at 41 kt with little change in central pressure height. The occluding process is evident with this low also.

On the fourth set (Figs. 16-19) we have magnified our field of numerical viewing to the details of the main low of grid 3. The low is now shown to have a course of about 070°, with a movement toward the east-northeast, at about 22 kt, and a deepening of 69 m, which is equivalent to about 9 mb. On this scale the thrust of warm air northward and cold air southward is the dominant feature on the temperature charts. Again, a small wave is shown on the trailing cold front.

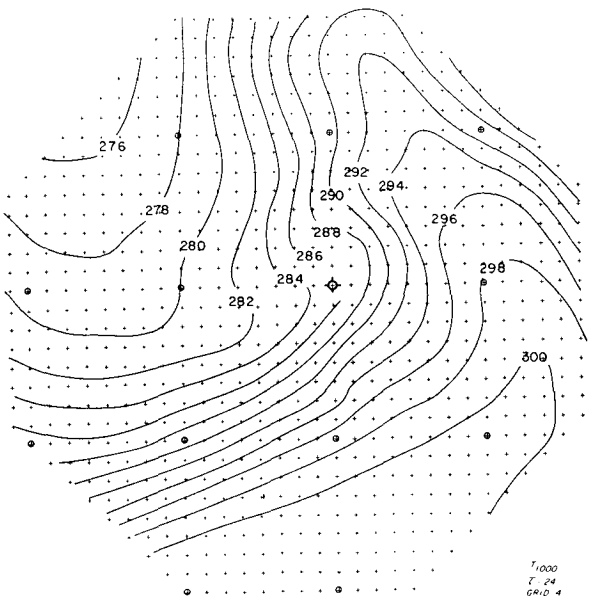

FIG. 19. 24-hr forecast 1000-mb temperature, grid 4.

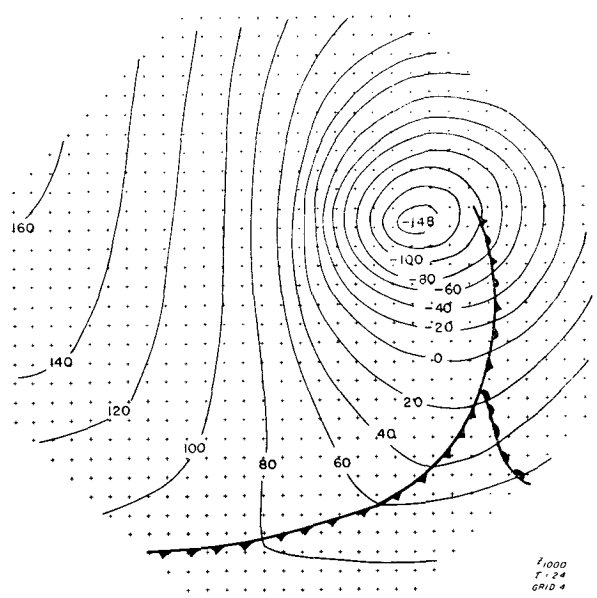

FIG. 21. Observed final ($\tau=24$) 1000-mb height, grid 4.

The final position of the warm and cold front near the center of the low is somewhat in question. Because the initial temperature data reflects the effect of several interpolations, the original frontal zone is not well depicted on this scale. Nevertheless, the main features of an intensifying low are obtained.

Finally, for the sake of general interest, the observed initial and final 1000-mb charts are shown in Figs. 20 and 21, respectively. The reproduction of these charts is based on weather charts of a 1:10,000,000 scale, which corresponds to the scale of grid 2 or perhaps between grid 2 and grid 3, so details actually present may be smoothed out. However, the movement, intensification and development of the disturbance are adequately given by these figures.

4. Conclusions

The results of our test case show that the method of grid telescoping can be successfully applied to a vorticity-type baroclinic model. Conditions along a boundary with either inflow or outflow can be predicted realistically. Twenty-four hour detailed predictions of a selected weather system are possible without having to maintain the same resolution over distant regions. It is noted that selection of the forecast region may depend upon the meteorological situation itself. Finally, we suggest that with the application of gird telescoping to more sophisticated models, such as those incorporating latent heat of condensation, parameterized convection, orographic effects, air-sea interaction or radiation, mesoscale numerical prediction may become practicable.

REFERENCES

Charney, J. G., R. Fjörtoft and J. von Neumann, 1950: Numerical integration of the barotropic vorticity equation. *Tellus*, **2**, 237–254.

Courant, R., K. Friedrichs and H. Lewy, 1928: Über die partiellen Differentialgleichungen der mathematischen Physik. *Math. Ann.*, **100**, 32–74.

Howcroft, J. G., 1966: Fine-mesh limited-area forecasting model. Tech. Rept. 188, U. S. Air Weather Service, 156 pp.

Richardson, L. F., 1922: *Weather Prediction by Numerical Process*. London, Cambridge University Press, 236 pp.

Shuman, F. G., 1957: Numerical methods in weather prediction: II—Smoothing and filtering. *Mon. Wea. Rev.*, **85**, 357–363.

Thompson, P. D., 1961: *Numerical Weather Analysis and Prediction*. New York, MacMillan Co., 170 pp.

——, and W. L. Gates, 1956: A test of numerical prediction methods based on the barotropic and two-parameter baroclinic models. *J. Meteor.*, **13**, 127–141.